9th Asia-Pacific Conference on Wind Engineering
Auckland, New Zealand
3-7 December 2017

Aerodynamic forces on two-dimensional rectangular cylinders subjected to accelerating flow: effect of side ratio

T. Yang[1], M. Mason[1]

[1]School of Civil Engineering
University of Queensland, Brisbane 4072, Australia

Abstract

The influence of flow acceleration on the aerodynamic forces applied to three two-dimensional rectangular cylinders was investigated through a series of unsteady wind tunnel tests. Experiments were performed on three rectangular cylinders with the same cross-wind depth, but differing along-wind length B. Side ratios of B/D = 1/3, 1 and 3 were tested over a Reynolds number (based on D) range of 9,200 to 102,000. The effect of side ratio and Reynolds number on unsteady aerodynamic loads were investigated. Results show that: (1) the applied flow acceleration has little effect on the aerodynamic loads on the short cylinder with B/D = 1/3; (2) there is a reduction in drag, fluctuating lift coefficients and Strouhal number after the start of flow acceleration for the square cylinder; (3) there is a reduction in peak lift coefficients for the elongated cylinder with B/D =3, but the Stouhal number is observed to increase. Physical mechanisms are proposed to explain the differences in experimental findings.

Introduction

Unsteady aerodynamics is of concern for wind engineers because winds commonly encountered by civil structures during severe wind storms are non-stationary in nature, i.e. the mean wind speed changes rapidly with time. For steady wind flow past two-dimensional cylinders, a considerable volume of research has shown that as wind speed varies, so too does vortex shedding frequency, drag and lift force [7,8]. A limited number of researchers have begun exploring whether similar relationships exist during unsteady winds [10-13]. For similar two-dimensional bodies subjected to rapidly accelerating flow conditions, an "overshooting" (i.e. an increase beyond what is expected under steady flow conditions) of drag and lift forces has been observed [10-13]. For one such case [13], it was found that the drag force on an inclined elliptic cylinder was increased by up to 50% over that observed in steady flow conditions when winds were accelerated from calm to 3.0m/s within 0.15s (i.e. an accelerating rate of 20m/s^2). More surprisingly, peak lift forces, increased by as much as 500% under these same conditions. If such extreme loads were to materialize during actual wind events, significant structural damage could occur at wind speeds well below design levels.

This paper explores the evolution of drag coefficients, fluctuating lift coefficients and dimensionless vortex shedding frequencies for two-dimensional bodies subjected to steady and accelerating flow conditions. Experiments were carried out in the actively controlled wind tunnel at the University of Queensland and resulting steady and unsteady loads on each body compared. Three two-dimensional rectangular cylinders were tested for a single flow acceleration rate so that the effect of side ratio could also be investigated.

Experimental setup and procedure

Experimental setup

Experiments were conducted in an open-circuit suck-down wind tunnel in the School of Civil Engineering at the University of Queensland. The test section has a cross-sectional area of 762mm ×762mm. When the test section is empty, the tunnel can reach wind speeds in excess of 40m/s with a freestream turbulence intensity of less than 0.5%.

Three rectangular cylinders were tested, each with the same cross-wind depth, D = 60mm, but differing along-wind lengths, B = 20, 60, 180mm. This results in three different side ratios, B/D = 1/3, 1 and 3, respectively. The resulting blockage ratio for each cylinder was 7.9%. No correction for potential blockage ratio effects were made for the present study.

Each cylinder was fixed at mid-height of the tunnel and restrained at the side walls (Figure 1) and positioned a distance of 0.5m into the test section and downwind of a 6:1 contraction section. Two circular end plates of 250mm diameter were fit to each model and symmetrically positioned 600mm apart. The centreline of each cylinder was circumferentially pressure tapped and fluctuating pressures measured. For each test a hotwire anemometer (Figure 1) measured instantaneous wind speeds above the cylinder, with its tip aligning to the windward face of each cylinder. Three pressure taps were mounted on the tunnel floor (Figure 1), below the windward face of each cylinder to measure the instantaneous reference static pressure. All velocity and pressure measurements were sampled at 600Hz with steady flow tests recorded for 190 seconds.

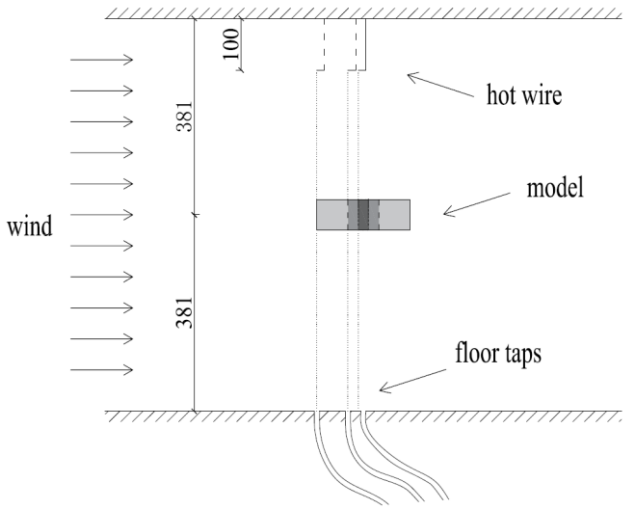

Figure 1. Experimental setup (Units: mm)

Experimental flow conditions

Accelerating flow conditions were generated in the test section by actively increasing the rotational speed of the wind tunnel fan

through an AC servomotor. One accelerating flow condition was tested on all cylinders, with 30 repeats run and results ensemble-averaged. Figure 2(a) shows the ensemble of wind speed time histories measured with the hotwire anemometer for all 30 runs. Excellent repeatability is seen from test to test. Each individual run was time aligned by assigning t = 0s to the midpoint between the start, U_s = 2.3m/s, and target, U_t = 25.5m/s, wind speeds. The instantaneous acceleration rate is obtained by calculating the velocity gradient between time steps +0.05s and -0.05s from the time of interest, Figure 2(b). The maximum acceleration rate is a = 14m/s^2, occurring at t = -0.19s, with a total acceleration period of 3.3s, as indicated by the asterisks in Figure 2(b).

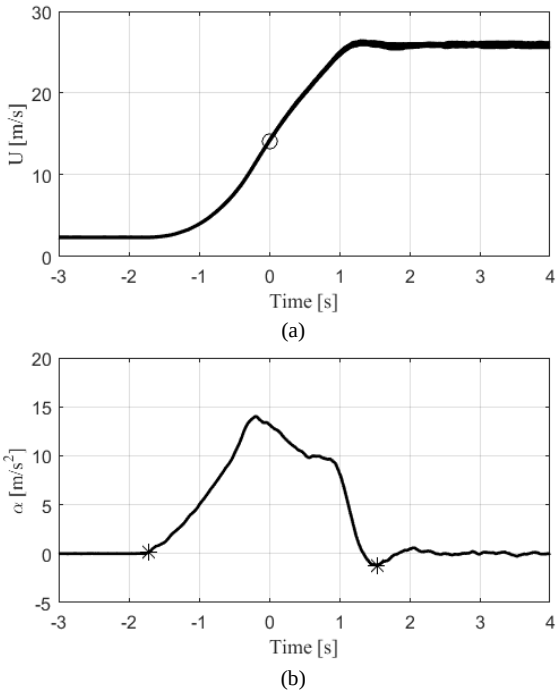

Figure 2. Time history of (a) velocity and (b) acceleration rate for accelerating flow tests in the present study. Time zero corresponds to the midpoint of start and target wind speed. Two asterisks in (b) indicate the start and end of acceleration period.

Data analysis procedure

All pressure data were corrected for tubing response distortion using the theoretical frequency response functions proposed by Bergh and Tijdeman (1965). Once corrected, these data were time aligned with reference velocities by assigning t = 0s to the first exceedance of $(U_s + U_t)/2$ in each velocity time history, and the first exceedance of $(P_{0s} + P_{0t})/4 + \sqrt{P_{0s}P_{0t}}/2$ in the pressure time history at the central tap of the windward face. P_{0s} and P_{0t} are the start and target net pressure, respectively.

Since all cylinders were placed at 0 ° angle of attack, instantaneous drag force time histories, $C_{D,t}(t)$, were calculated by integrated pressure over the windward and leeward faces, with lift force time histories, $C_{L,t}(t)$, calculated by integrated pressures on the top and bottom faces, Equations (1 & 2).

$$C_{D,t}(t) = \frac{\sum\left[\left(p_t(t) - p_s(\tilde{t})\right)\delta d\right]}{\frac{1}{2}\rho U(\tilde{t})^2 D} \quad (1)$$

$$C_{L,t}(t) = \frac{\sum\left[\left(p_t(t) - p_s(\tilde{t})\right)\delta d\right]}{\frac{1}{2}\rho U(\tilde{t})^2 B} \quad (2)$$

In these equations δd is the tributary area of each pressure tap and the tilde above t on both the static pressure and velocity signified that a moving average filtered (0.1s) time history was applied to minimize the influence of any localized fluctuations in these reference values.

Instantaneous Reynolds numbers, *Re*, were calculated for each time step of both the steady and accelerating flow tests, Equation (3).

$$Re = \rho UD/\mu \quad (3)$$

Here ρ is the air density, U the instantaneous wind speed, D the cross-wind depth and μ the dynamic viscosity of air. Reynolds number ranged from 9,200 to 102,000 for accelerating flow tests. Steady flow tests were run at 34 wind speeds ranging from 2.3m/s to 30.2m/s with corresponding time averaged Reynolds numbers of 9,200 < *Re* < 122,000.

Results and discussion

Evolution of drag coefficients with Reynolds number

The time evolution of instantaneous drag coefficients on the square cylinder, B/D =1, are shown in Figure 3. Each individual run is plot as a series of grey points, with the ensemble-average of these data, $< C_{D,t} >$, plot as a solid black line. For this example, a distinct drop of approximately 20% in drag coefficient is evident following the onset of flow acceleration.

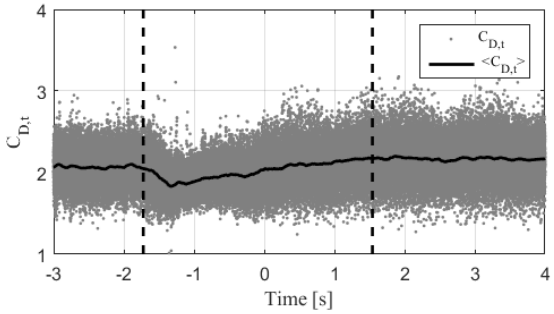

Figure 3. Time history of instantaneous and ensemble-averaged drag coefficients for the square cylinder, B/D =1, for all 30 runs. Two dashed lines indicate the acceleration period.

Ensemble-averaged drag coefficient, $< C_{D,t} >$, time histories for each of the three cylinders for the period of flow acceleration, i.e. between the dashed lines in Figure 3, are shown in Figure 4. Note that the X-axis has been transformed from time to instantaneous Reynolds number, as per Equation (3). Time-averaged drag coefficients measured during steady flow tests are also shown to facilitate the comparison between steady and unsteady results.

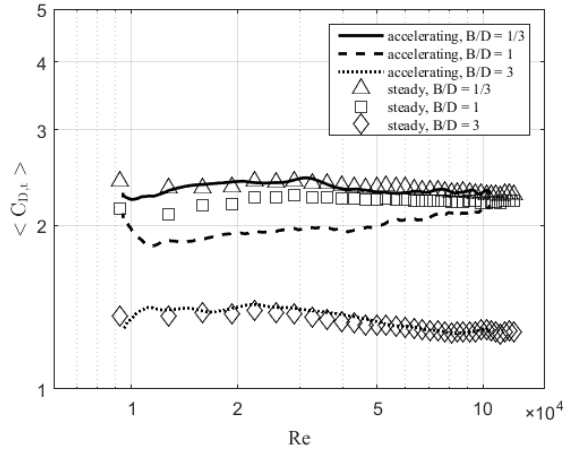

Figure 4. Ensemble-averaged and steady flow drag coefficients for the three cylinders as a function of instantaneous Reynolds number.

Figure 4 shows that the short cylinder (B/D = 1/3) experiences the highest drag coefficients, followed closely by the square cylinder, and the elongated cylinder (B/D =3) the lowest. This trend is true for both steady and accelerating flow conditions and for steady tests, agrees well with previous observations [3, 9].

For the rate tested, flow acceleration appears to have little effect on the drag coefficients of the short and elongated cylinders. This is evidenced by the fact that the accelerating flow drag coefficients follow steady flow test results closely throughout the entire *Re* range. However, drag coefficient for the square cylinder during accelerating flow are around 20% lower than during steady flow, and remain lower until the end of the acceleration period. This suggests that flow acceleration reduces the width of wake for this particular cylinder and acceleration rate. This appears not to be the case for either the short or the elongated cylinders.

Evolution of peak lift coefficients with Reynolds number

To evaluate the peak crosswind forces applied to each cylinder, peak fluctuating lift coefficients for each vortex shedding cycle were analysed. All positive and negative peaks were extracted for each lift coefficient time history (indicated by circles in Figure 5), and absolute values of adjacent positive and negative peaks were averaged. As a result, absolute peak lift coefficient, $|\hat{C}_{L,t}|$, time histories were generated for each run. Ensemble-averaged peak lift coefficients, $\langle|\hat{C}_{L,t}|\rangle$, were calculated by taking the average of all peaks within a moving window of 0.1s.

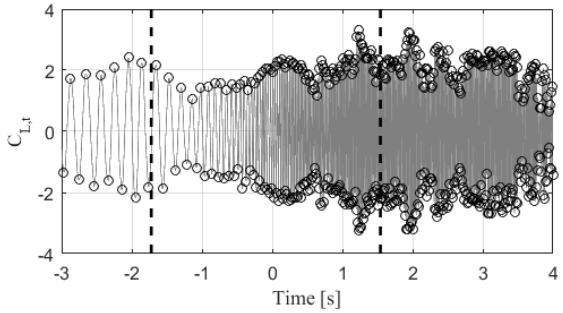

Figure 5. Time history of lift coefficients for the square cylinder under accelerating flow. Positive and negative peaks are marked by circles and two dashed lines indicate the acceleration period.

Following Figure 4, Figure 6 shows the variability of ensemble-averaged peak lift coefficients and time-averaged steady flow peak lift coefficients for each cylinder. Differing from drag coefficient observations, the largest steady flow lift coefficients are observed for the square cylinder. The short cylinder (B/D = 1/3) has the next highest, and the elongated cylinder again showing the smallest values. While not directly comparable, these trends agree with those previously reported for fluctuating lift coefficients by [9].

Flow acceleration is shown to have little effect on the peak lift coefficients for the short cylinder, with similar results observed for accelerating and steady flow tests across all Reynolds numbers. However, both the square and elongated cylinders show reduced lift coefficients (~40%) during the early stages of flow acceleration, but return to steady flow values prior to its cessation. Based on this observation it is hypothesised that in the early stages of flow acceleration the separated shear layers are supressed for the two longer cylinders. As flow ramping continues, these shear layers adapt to the instantaneous flow field and more closely resemble the steady flow cases.

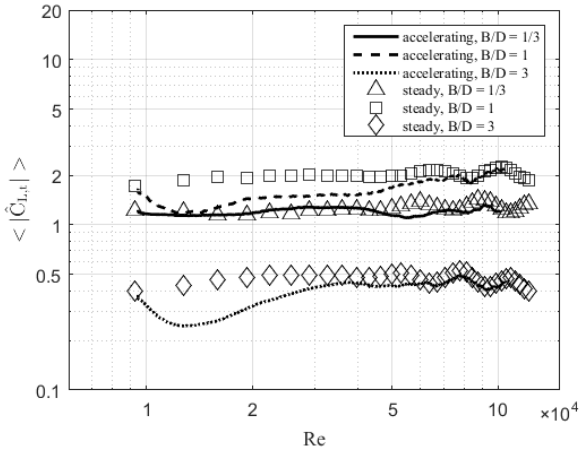

Figure 6. Ensemble-averaged and steady flow peak lift coefficients for the three cylinders as a function of Reynolds number

Evolution of Strouhal number with Reynolds number

The influence of flow acceleration on vortex shedding frequency (based on the dominant frequency of oscillating lift coefficients) was also examined. A Continuous Wavelet Transform (CWT), as used in previous studies of non-stationary wind signals [2, 4, 5], was used to determine time-dependent frequency information. A Morlet basis function was applied and the dominant frequency at each time step determined by finding the highest energy component in the wavelet scalogram. A frequency time history was thus generated for each test and transformed into a non-dimensional Strouhal number, S_t, time history using Equation (4).

$$S_t = fD/U \tag{4}$$

where f is the dominant frequency of lift coefficients derived from the CWT and *D* and *U* are as previously defined.

Figure 7 shows the ensemble-averaged, <*St*>, and time-averaged steady flow, *St*, Strouhal numbers for each of the three cylinders. The variation of *St* for steady flow tests show the opposite trend to the peak lift coefficients shown in Figure 6. That is, the highest *St* is found for the elongated cylinder, with the short cylinder and then square cylinder showing progressively lower values. This, again agrees with previous observations [9] and can intuitively be reasoned to imply that stronger vortices (i.e. larger imposed lifts forces) require longer to develop and therefore results in longer oscillation periods.

Figure 7 also shows that for accelerating flow cases, the ensemble-averaged Strouhal number for the short and elongated cylinders increases slightly during the early stage of acceleration. It then returns back to its steady-state value by Re= 30,000. This implies that the flow acceleration strengthens the interaction of vortices for these two cylinders, and at least for the elongated cylinder, corresponds to a decrease in peak lift coefficients over that period.

For the square cylinder, Figure 7 shows a decrease in Strouhal number below its steady flow values over the entire Re range. This observation suggests that the flow acceleration inhibits the interaction of vortices for this cylinder, but given Figure 4 and 6 also show significant differences to steady results, this may not be quite as straightforward. Future flow visualization tests will seek to understand the interaction between flow acceleration and wake dynamics in greater detail.

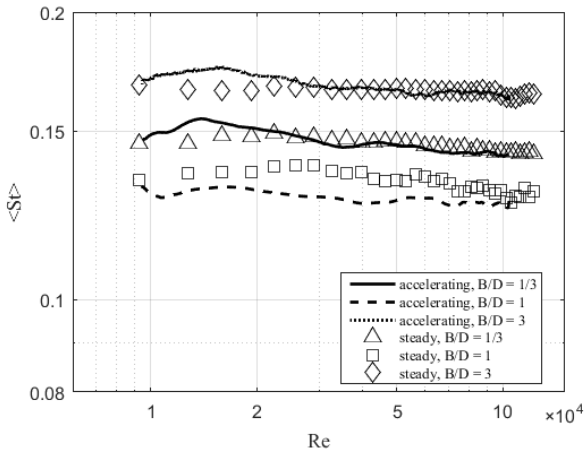

Figure 7. Ensemble-averaged and steady flow Strouhal number for the three cylinders as a function of Reynolds number.

Conclusions

Steady and accelerating flow wind tunnel tests were carried out to investigate the influence of flow acceleration on aerodynamic loads on three two-dimensional rectangular cylinders. For accelerating flow tests wind speed ramped from 2.3 to 25.5m/s within 3.3s, with a peak acceleration rate of 13 m/s^2 and a corresponding *Re* range of 9,200-102,000. Thirty repeat tests were conducted for each cylinder configuration and ensemble-averaged results were compared with steady flow test results. The main conclusions are summarized as follows:

(1) Unlike for the tests reported by [10-13], no overshoot of either drag or lift force coefficients were observed for the current test configuration. This is believed to be the case because those previous experiments were carried out at lower wind speeds than tested here, thus allowing inertial forces to play a greater role in wind loading. Moving forward it will be important to ensure such forces are scaled appropriately when drawing conclusions about wind loading of full-scale structures.

(2) For the rate tested, flow acceleration has little effect on the aerodynamic loads on the short cylinder (B/D =1/3). When comparing ensemble-averaged drag coefficients and lift coefficients with steady flow results, little observable difference was found. However, a slight increase in the Strouhal number immediately after the start of acceleration was observed, and the cause of this deserves further investigation.

(3) Flow acceleration has an inhibiting effect on the aerodynamic loads on the square cylinder (B/D=1), with reduced drag coefficients, fluctuating lift coefficients, and Strouhal numbers observed. This was true for much of the period of acceleration, with values only returning to their steady flow magnitudes once acceleration ceases. It is hypothesised that with the addition of external acceleration, the shear layers around the side faces are supressed to an extent that the wake is narrower and more symmetrical.

(4) Flow acceleration had an inhibiting effect on crosswind forces felt by the elongated cylinder (B/D=3). However, for the early period of the acceleration ramp, enhanced shedding frequencies were observed. Little influence on drag force coefficients were noted when compared with steady flow tests.

Flow visualisation tests may shed more light on the physical mechanisms behind some of the observed deviations from steady flow results observed during periods of flow acceleration. Tests on a wider range of bodies and over a wide range of flow acceleration (and deceleration) cases are still required before firm conclusions can be drawn about the relative importance of flow acceleration for wind engineering of structures during severe windstorms.

Acknowledgments

The authors would like to acknowledge the funding for this project made available through The University of Queensland Grant, NS-1501.

References

[1] Bergh, H., & Tijdeman, H. (1965). Theoretical and experimental results for the dynamic response of pressure measuring systems.

[2] Gurley, K., & Kareem, A. (1999). Applications of wavelet transforms in earthquake, wind and ocean engineering. Engineering structures, 21(2), 149-167.

[3] Holmes, J. D. (2015). Wind loading of structures. CRC press.

[4] Indrusiak, M. L. S., Goulart, J. V., Olinto, C. R., & Möller, S. V. (2005). Wavelet time–frequency analysis of accelerating and decelerating flows in a tube bank. Nuclear engineering and design, 235(17), 1875-1887.

[5] Kareem, A., & Kijewski, T. (2002). Time-frequency analysis of wind effects on structures. Journal of Wind Engineering and Industrial Aerodynamics, 90.

[6] Norberg, C. (1993). Flow around rectangular cylinders: pressure forces and wake frequencies. Journal of wind engineering and industrial aerodynamics, 49(1-3), 187-196.

[7] Okajima, A. (1982). Strouhal numbers of rectangular cylinders. Journal of Fluid Mechanics, 123, 379-398.

[8] Roshko, A. (1954). On the drag and shedding frequency of bluff cylinders. NACA TN, 3169

[9] Sohankar, A. (2008). Large eddy simulation of flow past rectangular-section cylinders: Side ratio effects. Journal of wind engineering and industrial aerodynamics, 96(5), 640-655.

[10] Takeuchi, T., Maeda, J., & Kawashita, H. (2008). The overshoot of aerodynamic forces on a railcar-like body under step-function-like gusty winds. In Sixth International Colloquium on Bluff Body Aerodynamics & Applications, Milano, July (pp. 20-24).

[11] Takeuchi, T., Maeda, J., Hayata, T., & Kawashita, H. (2009). Effects of section size on aerodynamic forces on an elliptic cylinder under short-rise-time gusts. Proc. of APCWE VII.

[12] Takeuchi, T., & Maeda, J. (2010). Effects of inertia force proportional to flow acceleration on unsteady wind forces acting on an elliptic cylinder under short-rise-time gusts. In Proceedings of 5th International Symposium on Computational Wind Engineering.

[13] Takeuchi, T., Maeda, J., & Otsubo, K. (2013). Numerical and experimental investigations on unsteady wind. In Proceedings of 8th Asia-Pacific Conference on Wind Engineering (pp. 795-798).